JOURNAL OF MATERIALS SCIENCE 24 (1989) 1195–1202

Preparation and characterization of precursor powders for yttria-doped tetragonal zirconia polycrystals (Y-TZP) and Y-TZP–Al_2O_3 composites

S. RAJENDRAN, H. J. ROSSELL, J. V. SANDERS
CSIRO, Division of Materials Science and Technology, Locked Bag 33, Clayton, Victoria 3168, Australia

Precursor powders for the preparation of tetragonal 2.5 mol % Y_2O_3–ZrO_2 containing 0 to 30 wt % Al_2O_3 were made by coprecipitation. The behaviour of this powder during calcination from room temperature to 1200° C was studied using differential thermal analysis, X-ray diffraction and transmission electron microscopy methods, and measurements of surface area. The uncalcined powder was essentially amorphous. On heating alumina-free powder, zirconia crystallized at 485° C: for increasing alumina content, zirconia crystallized from an amorphous aluminous matrix at increasing temperatures (850° C for 20 wt % Al_2O_3), while the crystallite size decreased and the surface area of the powder increased. The zirconia first crystallized as cubic, but transformed to the tetragonal form near 1100° C. The alumina crystallized as corundum at 1200° C. No monoclinic zirconia could be detected when calcined aluminous material was cooled to room temperature. The sintering behaviour of the calcined powder is discussed.

1. Introduction

Partially stabilized zirconia (PSZ) is zirconia containing an amount of stabilizer that is insufficient to convert the whole to the cubic form; by suitable heat treatment, the unstabilized portion can appear as precipitate of metastable tetragonal zirconia. This material is stronger and tougher than fully stabilized cubic zirconia. The improvement in strength and toughness has been explained as due to the shape and volume change of the tetragonal zirconia precipitates during a stress-induced transformation to the stable monoclinic form [1]. Such "transformation toughening" has been used in the development of a number of engineering ceramics [2–4], and for improvement of the strength and toughness of alumina in particular [2, 5, 6].

Lange [7] reported that improved strength and toughness could be achieved for a ceramic containing equal quantities of tetragonal ZrO_2 and α-Al_2O_3. Tsukuma and Ueda [8] reported a strength of about 2.4 GPa for composites of tetragonal ZrO_2/3 mol % Y_2O_3 (Y-TZP) with $\geqslant$ 20 wt % Al_2O_3 after hot isostatic pressing (HIPing). This represents a large improvement in the strength of Y-TZP; however, the role of alumina in this improvement is unclear.

In an attempt to provide data on the influence of alumina on Y-TZP materials, composites of zirconia–2.5 mol % yttria with 0 to 30 wt % alumina were fabricated from coprecipitated gels of hydrated oxides. It was observed that the addition of alumina greatly influenced the electrical and mechanical properties of the finished Y-TZP material [9, 10]. In this paper, the preparation and characterization of the coprecipitated powders are reported.

2. Experimental procedure

Solutions of yttrium and zirconium, prepared by dissolving 99.9% yttria and zirconium oxycarbonate in AR nitric acid, were standardized and mixed in proportions corresponding to 0.025 Y_2O_3–0.975 ZrO_2. Appropriate proportions of this solution and of a stock solution of AR aluminium nitrate in distilled water were mixed and added with stirring to AR ammonia solution to produce a coprecipitate of hydrated oxides. The pH of the solution before and after the precipitation was maintained at 12.0 and 9.0, respectively. The precipitate was filtered, washed free from nitrate, ultrasonically dispersed in acetone for an hour twice, then dried in a vacuum oven at 75° C for 24 h. The precipitation, filtration and washing were done under nitrogen to prevent peptization or compositional alteration of the precipitate that could result if the pH was lowered because of absorption of atmospheric CO_2.

Differential thermal analyses (DTA) of the specimens with simultaneous thermogravimetry (TG) were made using a Stanton Redcroft Derivatograph. The temperature range was 20 to 1400° C, the heating rate 20° C min^{-1}, and the specimen size 20 mg.

Powder X-ray diffraction patterns were recorded using a Rigaku diffractometer and filtered Cu$K\alpha$ radiation. A scanning rate of 2° min^{-1} was used to obtain patterns for phase analysis, and $\frac{1}{2}$° min^{-1} for crystallite size estimations. Particle sizes for the

0022–2461/89 $03.00 + .12

zirconia phase were estimated from the widths of the (1 1 1) diffraction peak (20 to 30°), using the Scherrer equation. Instrumental broadening was a relatively small effect, and no correction for this was applied.

Diffraction patterns of some specimens were recorded on film using a Guinier–Lenné focusing camera operating with Cu$K\alpha_1$ radiation. This device produces a continuous record of the diffraction pattern as the specimen is heat treated according to a desired programme in the range 20 to 1500° C. Specimens were prepared by painting a slurry of the material in acetone on to a platinum support mesh: diffraction lines from the platinum sometimes appeared, but were unobjectionable. Thoria was used as an internal standard: the variation of its lattice parameter with temperature was taken to conform with the expression

$$a/a_0 = -0.179 + 5.097 \times 10^{-4}T + 3.732 \times 10^{-7}T^2 - 7.594 \times 10^{-11}T^3,$$
$$150 \leqslant T \leqslant 2000\,\text{K} \quad [11]$$

and using $a_0 = 0.559\,72$ nm at 293 K.

Transmission electron microscopy was done with a Jeol 100CX microscope operating at 100 kV. Samples for TEM were prepared by allowing an aqueous suspension to dry on grids coated with carbon film.

Specific surface area measurements were made by the BET method using nitrogen adsorption at − 193° C after initial outgassing of the samples at 200° C overnight: the instrument was a "sorptomatic" model (Carl Erba, Italy).

3. Results

The nomenclature ZY*XX*Al_2O_3-*t* used here refers to composite materials of zirconia–2.5 mol % Y_2O_3 with *XX* wt % Al_2O_3, heated for 2 h at temperature *t*° C.

Fig. 1 contains typical DTA curves for the oven-dried coprecipitated hydrated oxides. All the curves show a broad endotherm at about 160° C and an exotherm at a higher temperature. The temperature of the latter increases from 485 to 920° C as the alumina content of the specimen increases from 0 to 30 wt %. In addition, aluminous specimens (curves 2 to 5) show an additional endotherm that lies between the endotherm and exotherm mentioned above, and which increases in size and shifts to lower temperatures as the alumina content of the specimens increases.

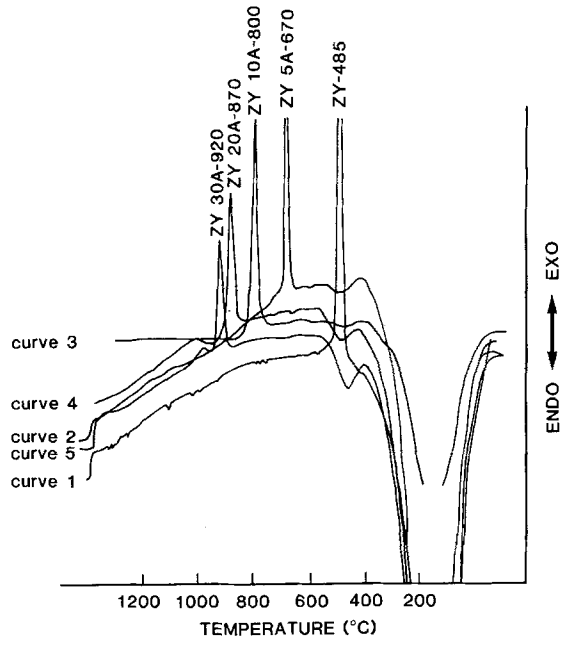

Figure 1 Differential thermal analysis (DTA) curves of oven dried Y_2O_3–ZrO_2 and Y_2O_3–ZrO_2–Al_2O_3 samples.

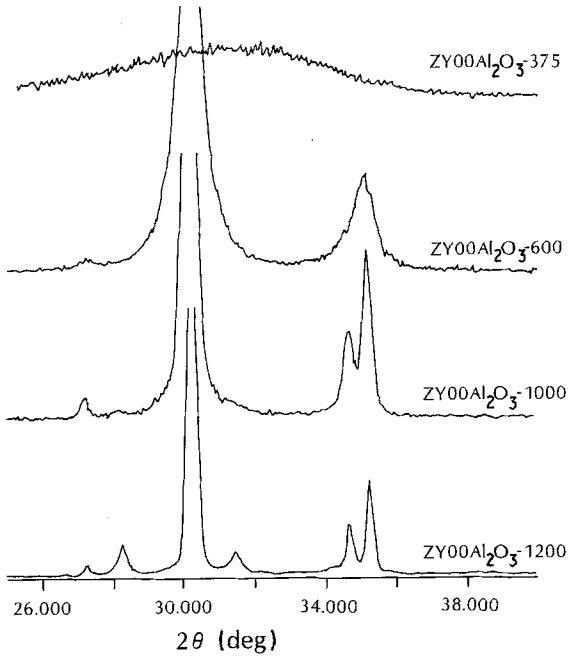

Figure 2 Room temperature X-ray diffraction patterns of precipitated Y_2O_3–ZrO_2 specimens that had been calcined at temperatures from 375 to 1200° C.

Room-temperature X-ray diffraction patterns of alumina-free specimens that had been calcined at temperatures from 375 to 1200° C (ZY-375, ZY-600, . . .) for 2 h are given in Fig. 2. The specimen ZY-375 was amorphous to X-rays, while crystalline tetragonal zirconia with small amounts ($\leqslant$ 5 wt %) of monoclinic zirconia appears in ZY-600 and remaining specimens. Specimens ZY*XX*Al_2O_3-600 were all amorphous to X-rays with the exception of ZY5Al_2O_3-600, which was crystalline, with a powder pattern similar to that of ZY-600. The powder X-ray diffraction patterns of the ZY*XX*Al_2O_3-1000 specimens (Fig. 3) all showed the presence of the crystalline tetragonal zirconia phase: there was no X-ray diffraction evidence for the presence of any monoclinic zirconia, or for any crystalline alumina. The first X-ray diffraction evidence for alumina appeared in the patterns for specimens ZY*XX*Al_2O_3-1200, when peaks due to α-alumina (corundum) could be seen.

A Guinier–Lenné photograph of ZY20Al_2O_3 heated from room temperature to 1300° C at 50° C h^{-1} and cooled after 1 h at 100° C h^{-1} (film speed 1.5 mm h^{-1}) is shown in Fig. 4. This photograph is particularly revealing. Thus, as the specimen is heated from room temperature to 800° C, no diffraction lines due to crystalline material appear, but there is a notably increased background intensity due to scattering from amorphous, or cryptocrystalline material. At 850° C, the high background reduces abruptly as the scattering becomes concentrated into broad lines due to very

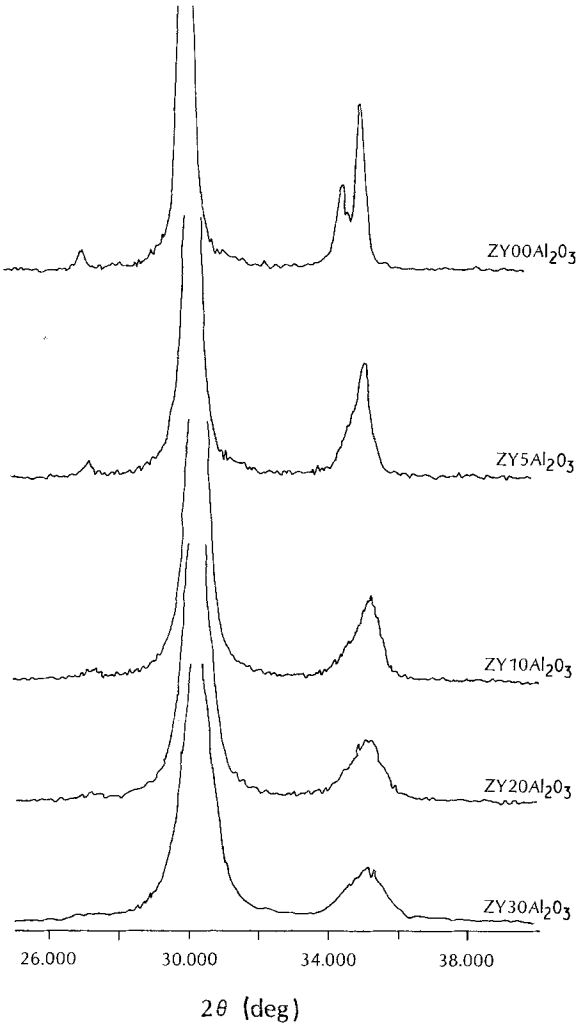

Figure 3 Room temperature powder X-ray diffraction patterns of Y_2O_3–ZrO_2 and Y_2O_3–ZrO_2–Al_2O_3 specimens calcined at 1000° C.

small crystals of cubic zirconia. A microdensitometer record of the first four zirconia lines was made, from which an estimate of 12.5 ± 1.5 nm for the crystallite size was obtained using the Scherrer equation, and value of 0.5140 nm determined for the lattice parameter at 900° C. At about 900° C, the crystallites begin to grow, as shown by a narrowing of the diffraction lines, and they are about 100 nm (the limit of the line-broadening estimation) by 1130° C. The cubic zirconia phase transforms to the tetragonal form at 1010° C, and this modification persists even after the specimen is cooled to room temperature: the monoclinic form of zirconia does not appear at any stage. Diffraction lines from corundum appear at 1180° C. This is the first diffraction evidence for any alumina phase: the diffraction lines are faint because of the relatively small scattering power and low weight fraction of alumina, nonetheless it would be expected that diffraction lines from crystalline forms of alumina or its hydrates would be visible below 1180° C had these forms been present in the specimen.

Fig. 5 shows typical TEM images of alumina-free specimens that had been calcined in the range 375 to 1200° C for 2 h. The ZY-375 material has a sponge-like structure. The corresponding electron diffraction pattern showed only a faint diffuse ring indicating that there is no crystalline ordering larger than about 0.2 nm. The ZY-600, ZY-1000 and ZY-1200 specimens are composed of angular crystallites of about 20, 50 and 120 nm diameter, respectively. The corresponding electron diffraction patterns show diffraction spots in the positions expected for cubic or tetragonal zirconia: no distinction can be made because of the somewhat spread nature of the spots and the inherently low resolution of the patterns.

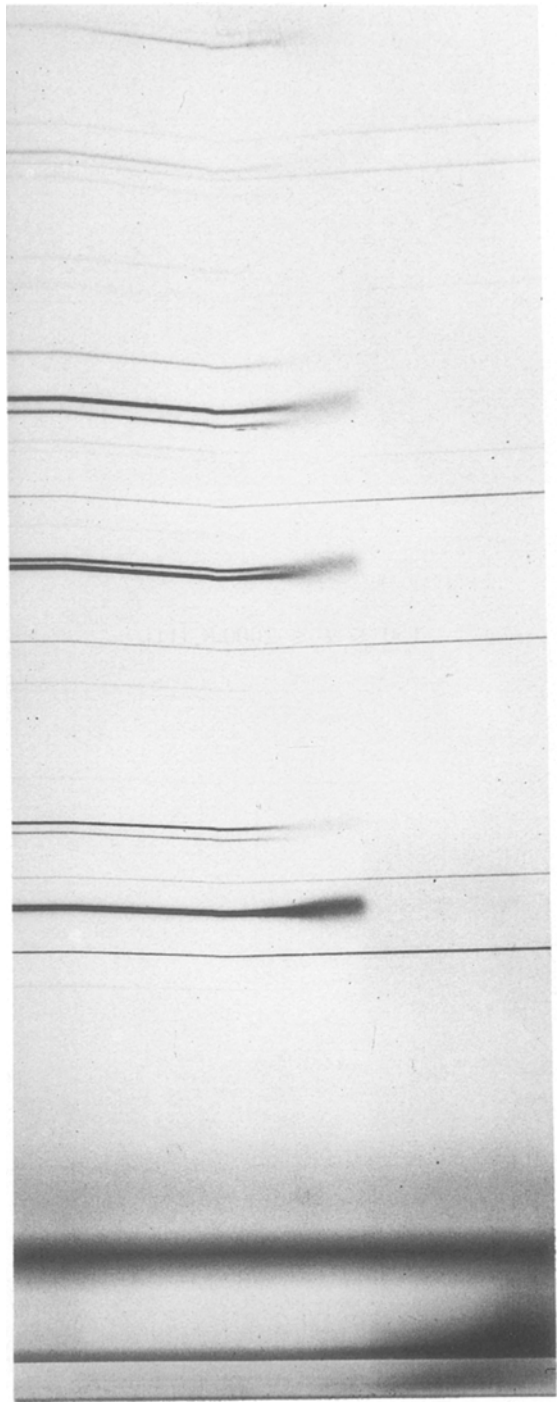

Figure 4 Guinier–Lenné photograph of a $ZY20Al_2O_3$ sample heated from 50 to 1300° C and cooled.

Electron diffraction patterns from aluminous specimens calcined at 600° C showed spots due to zirconia crystallites only in the case of $ZY5Al_2O_3$-600; the remainder were amorphous. Dark-field images of ZY-600 and $ZY5Al_2O_3$-600 formed with beams corresponding to the sharp diffraction spots (Fig. 6) reveal some of the crystallites present in these materials. TEM images from aluminous specimens calcined at

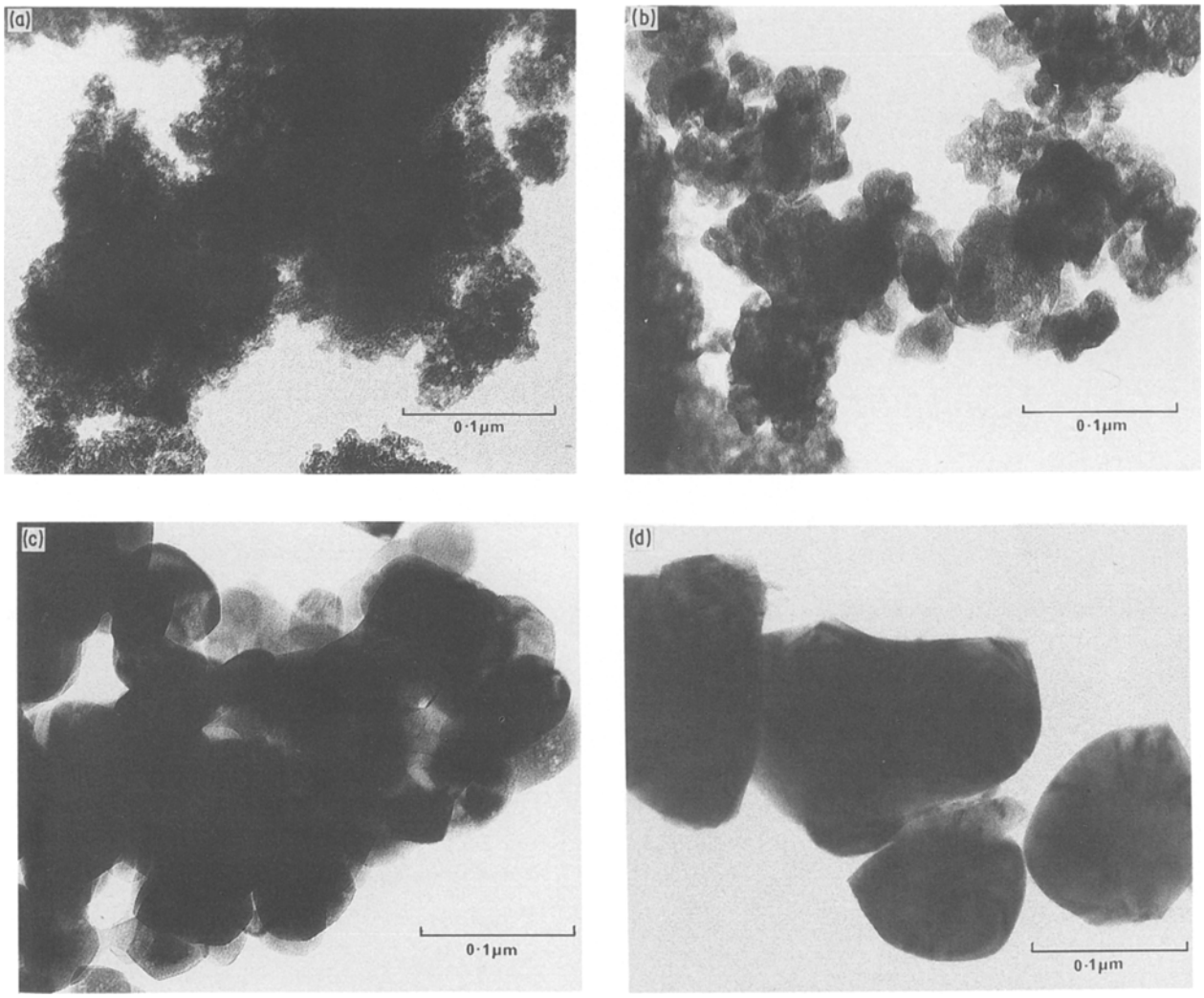

Figure 5 Transmission electron micrograph of Y_2O_3–ZrO_2 specimens calcined previously at (a) 375, (b) 600, (c) 1000 and (d) 1200° C, for 2 h.

1000° C showed that crystallites were present in all cases, and that there was a notable reduction in the size of these crystallites as the alumina content increased (Fig. 7). The corresponding electron diffraction patterns showed rings of spots as expected for cubic or tetragonal zirconia, with the rings becoming smoother and less spotty as the alumina content of the specimen increased, an effect due to the inclusion of an increasing number of crystallites (and therefore of crystallite orientations) in the area selected for diffraction as the crystallite size decreased.

The electron diffraction patterns from aluminous specimens that had been calcined at 1200° C (Fig. 8) all showed rings of spots as expected for tetragonal zirconia. Rings of spots corresponding to α-alumina (corundum) also appeared, with intensities that increased as the alumina content of the specimen increased. The TEM images showed that the

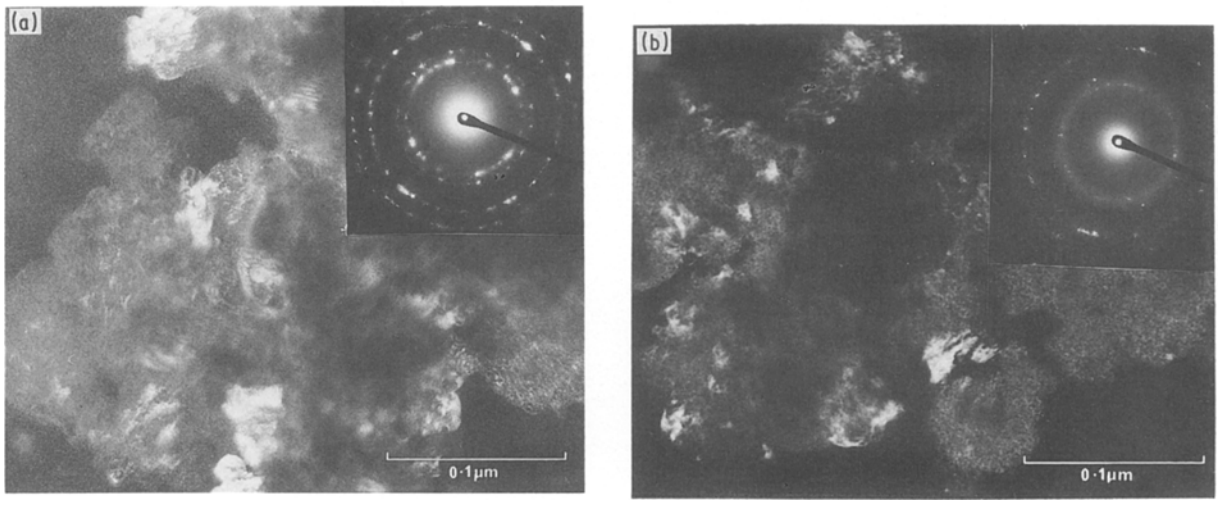

Figure 6 Dark-field images and electron diffraction patterns of (a) $ZY00Al_2O_3$-600 and (b) $ZY05Al_2O_3$-600° C specimens.

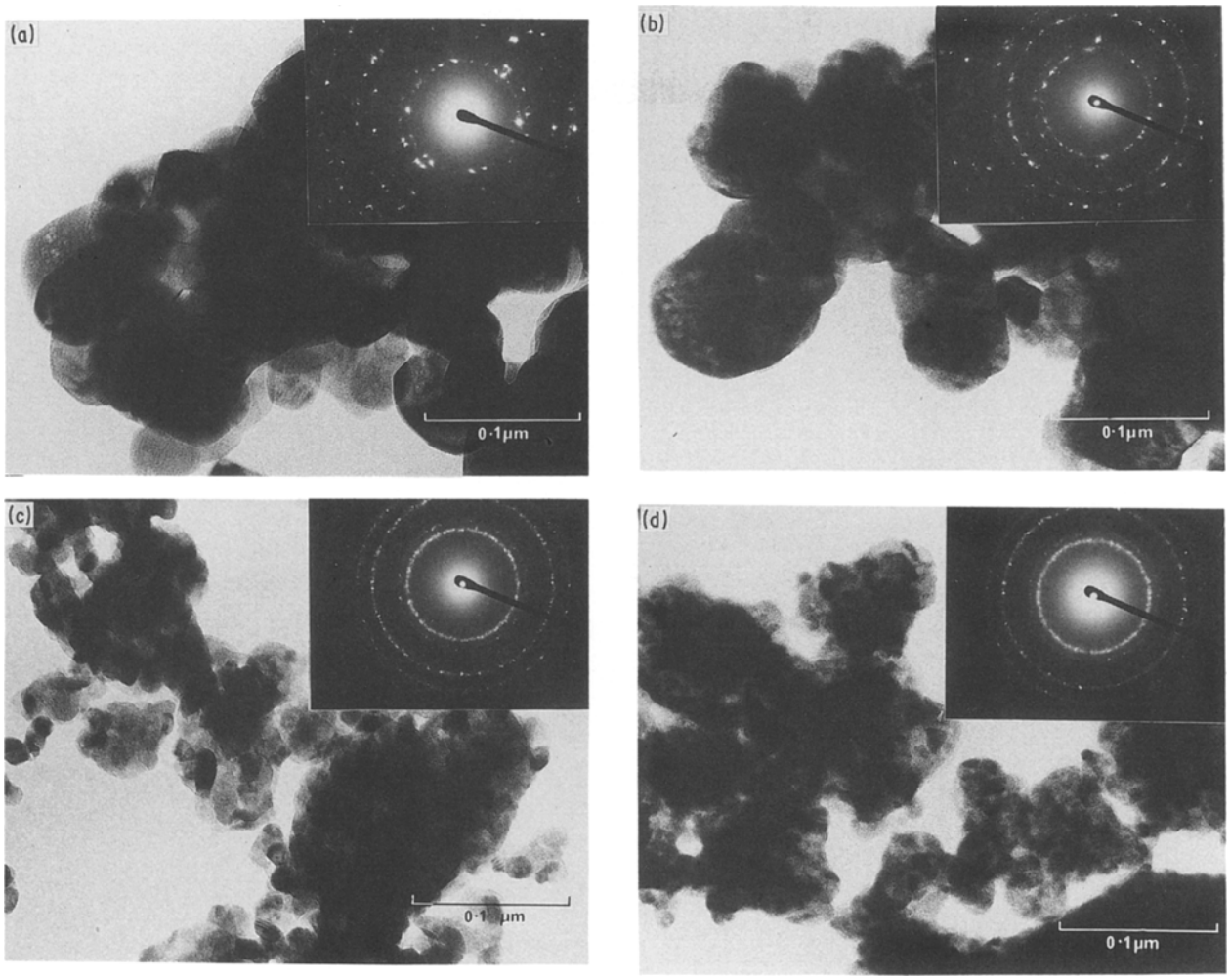

Figure 7 Transmission electron micrographs and electron diffraction patterns of $ZYXXAl_2O_3$-1000 specimens, (a) $ZY00Al_2O_3$, (b) $ZY05Al_2O_3$, (c) $ZY10Al_2O_3$, (d) $ZY20Al_2O_3$ and (e) $ZY30Al_2O_3$.

crystallites of both phases were of similar sizes in any one $ZYXXAl$-1200 specimen, that these crystallite sizes were about twice those seen in images from $ZYXXAl$-1000 specimens of corresponding alumina content, and that the crystallite size in $ZYXXAl$-1200 specimens decreased from about 100 to 50 nm as the alumina content rose from 5 to 30 wt %.

Specific surface areas of ZY and $ZYXXAl_2O_3$ specimens calcined at different temperatures are given in Table I. A notable reduction in the specific surface area of ZY material occurs between 375 and 600° C, but there is only a gradual decrease after calcination at higher temperatures. In the case of $ZYXXAl_2O_3$ specimens calcined at any given temperature, the surface area increases with increasing alumina content.

Particle sizes estimated from X-ray line broadening for the zirconia phase in various specimens are given in Table II. No attempt was made to determine particle sizes to a high degree of precision. The values probably are correct to about 10%, and represent a useful confirmation of the particle sizes obtained from TEM images, where only very small quantities of specimen are examined.

4. Discussion

The broad endotherm appearing at relatively low temperatures for all the DTA curves of Fig. 1, is associated with a weight loss, and must be due to the removal of loosely bound and constitutional water from the hydrated gels. The second, smaller endotherm appearing in the aluminous specimens is

TABLE I Surface area ($m^2 g^{-1}$) of the samples calcined to different temperature

Samples	Calcination temperature (° C) (2 h)			
	375	600	800	1000
$ZY00Al_2O_3$	212	79	49	22
$ZY05Al_2O_3$	–	85	–	27
$ZY10Al_2O_3$	–	136	–	33
$ZY20Al_2O_3$	–	151	–	41
$ZY30Al_2O_3$	–	185	–	53

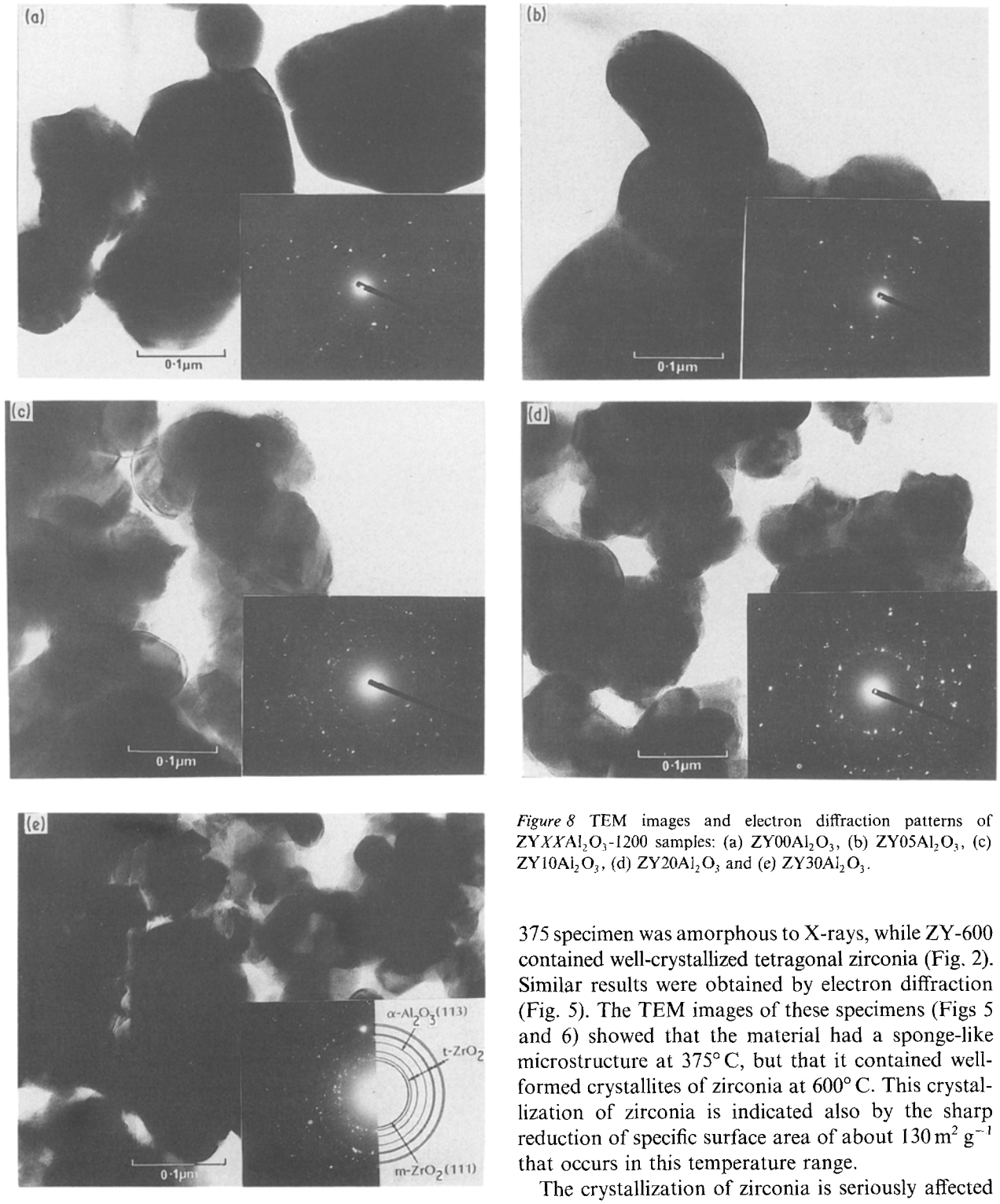

Figure 8 TEM images and electron diffraction patterns of $ZYXXAl_2O_3$-1200 samples: (a) $ZY00Al_2O_3$, (b) $ZY05Al_2O_3$, (c) $ZY10Al_2O_3$, (d) $ZY20Al_2O_3$ and (e) $ZY30Al_2O_3$.

also associated with a weight loss, and its magnitude increases as the proportion of alumina present increases. It is probable that this endotherm is due to dehydration of an alumina species. Calculations based on the TG results indicated that the endotherm was due to the formation of Al_2O_3 from an AlOOH species rather than from $Al(OH)_3$. The formation of Al_2O_3 from AlOOH is usually associated with an endotherm at about 500° C [12]. In the present case, however, the alumina species involved could not be identified by X-ray or electron diffraction, nor by infrared spectroscopy.

It is evident that the sharp exothermic peak in each DTA curve for temperatures above 480° C is due to the crystallization of zirconia. Thus, the ZY-375 specimen was amorphous to X-rays, while ZY-600 contained well-crystallized tetragonal zirconia (Fig. 2). Similar results were obtained by electron diffraction (Fig. 5). The TEM images of these specimens (Figs 5 and 6) showed that the material had a sponge-like microstructure at 375° C, but that it contained well-formed crystallites of zirconia at 600° C. This crystallization of zirconia is indicated also by the sharp reduction of specific surface area of about $130\,m^2\,g^{-1}$ that occurs in this temperature range.

The crystallization of zirconia is seriously affected by the presence of alumina in the specimens. Thus, as shown by the exothermic DTA peaks, there is a systematic increase in the temperature at which zirconia crystallizes, and a reduction in the energy of crystallization per unit mass as the alumina content increases.

TABLE II Particle size (nm) of the zirconia phase in various specimens calcined at 1000 and 1200° C

Samples	Calcination temperature (° C) (2 h)	
	1000	1200
$ZY00Al_2O_3$	28	43
$ZY05Al_2O_3$	21	44
$ZY10Al_2O_3$	15	41
$ZY20Al_2O_3$	11	39
$ZY30Al_2O_3$	9	36

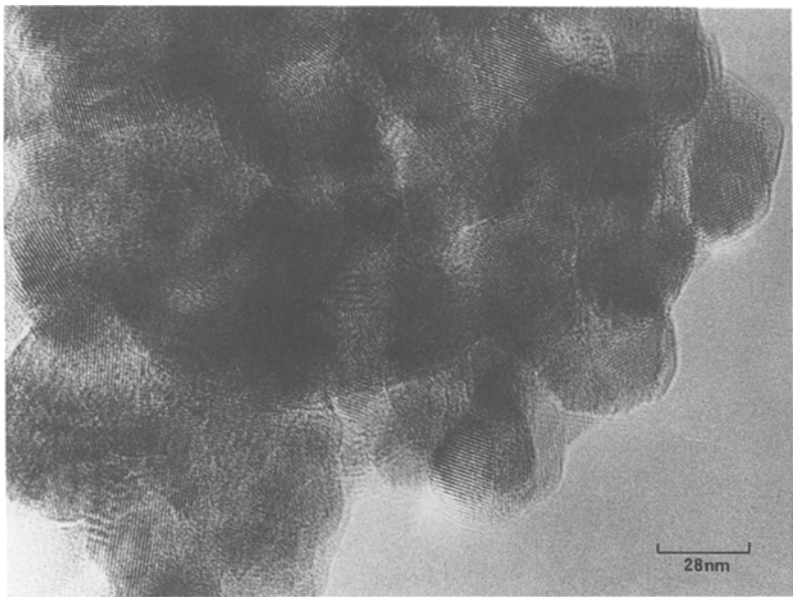

Figure 9 High-resolution TEM image of ZY30Al_2O_3-1000 specimen.

Also, the TEM and specific surface area results show that the zirconia crystallites formed at 1000° C are smaller for increasing alumina content.

These results are explicable if it is assumed that the zirconium and aluminium are uniformly distributed in the amorphous powder at low temperature. Then, at higher temperatures, the nucleation and growth of zirconia crystallites would be controlled by diffusion of zirconium (and yttrium) in this amorphous material, the smaller crystallites produced in a fixed time at higher alumina contents being a consequence of the increasing dilution of the zirconia. The amorphous phase left behind would be alumina-rich. This interpretation is supported by the TEM images of ZY30Al_2O_3-1000 (Fig. 9) in which it can be seen that the zirconia crystallites are coated by, or are embedded in, some matrix material, which could well be alumina: as noted above, the alumina present in any sample could not be detected or identified until corundum crystals were produced by calcination at 1200° C.

It is unlikely that the change of crystallization behaviour of zirconia as the alumina content changes is due to solid solution of alumina in the zirconia: there was no change in the lattice parameters of the zirconia phase for different alumina contents, while the solid solubility of alumina in zirconia is reported to be very limited [13].

The materials containing $> 5\%$ Al_2O_3 described

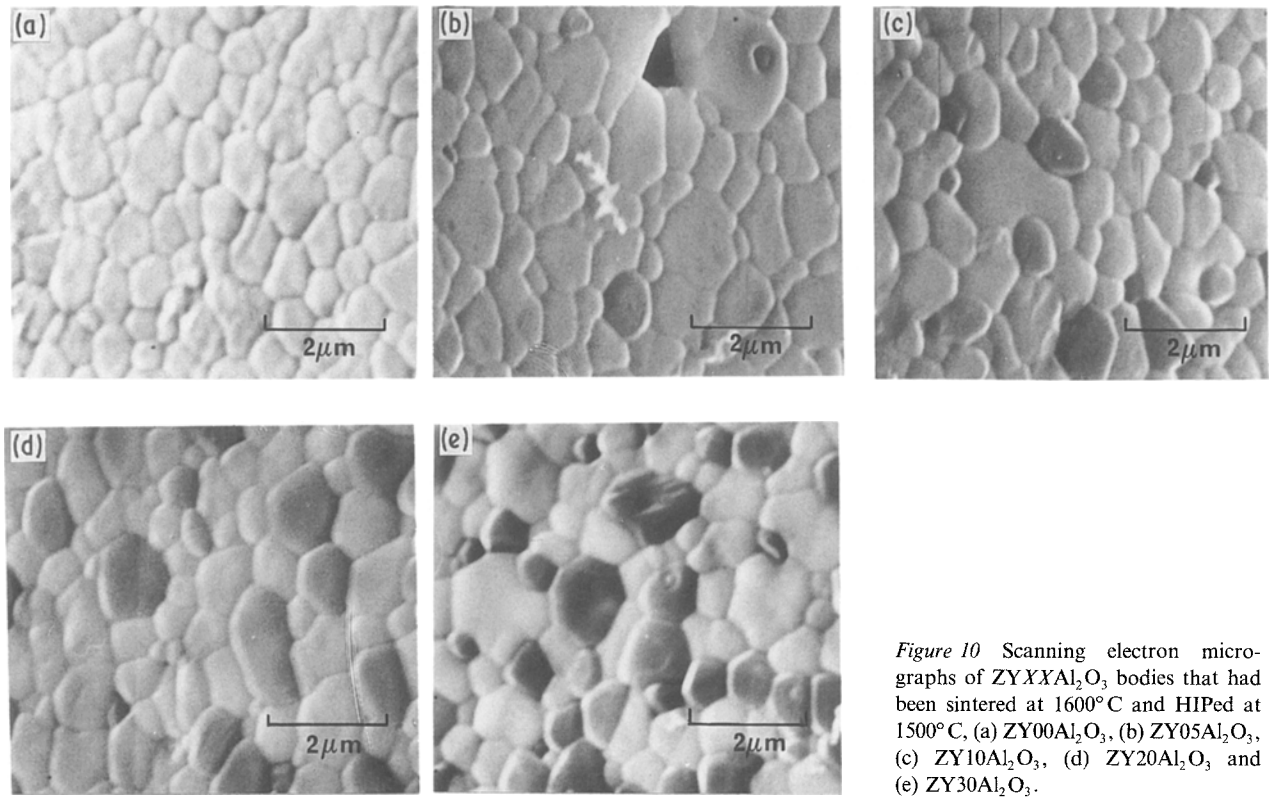

Figure 10 Scanning electron micrographs of ZY*XX*Al_2O_3 bodies that had been sintered at 1600° C and HIPed at 1500° C, (a) ZY00Al_2O_3, (b) ZY05Al_2O_3, (c) ZY10Al_2O_3, (d) ZY20Al_2O_3 and (e) ZY30Al_2O_3.

here can be sintered close to theoretical density by a short heat treatment at 1500° C, as reported elsewhere [10]. This temperature is about 200° C lower than that usually required to sinter zirconia materials. The resulting ceramic has extremely high strength (> 2 GPa), the origin of which lies partly in the microstructure (Fig. 10). Here, tetragonal zirconia phase is present as small approximately equiaxed crystals of about 1 μm size, and there is a uniform dispersion of alumina as similarly-sized corundum crystals. Also, there appears to be no intergranular phases, because these materials possess notably low grain-boundary resistivity [9].

The role of the alumina in the development of this highly desirable microstructure has not been established. It is probable that in the initial stages of calcination, the very uniform dispersion of zirconia crystallites nucleates and grows in an amorphous alumina matrix phase, which controls the necessary diffusion. Also, it is clear that the approximately uniform crystals of zirconia and alumina observed in the finished ceramic could well evolve from the dispersion of equally-sized crystallites present at 1200° C by the expected processes of ripening and grain growth. However, it is not clear whether the alumina plays any part in the excellent sintering behaviour of these materials, or whether this is simply a consequence of the well-dispersed, equally sized crystallites present at presintering temperatures. The alumina present as well-dispersed crystallites of 100 nm diameter at 1200° C must migrate relatively large distances in forming the dispersion of 1 μm crystals seen in material sintered at 1600° C: this migration most probably occurs in grain boundaries. It may be speculated that the very clean grain boundaries that give rise to the desirable properties of these ceramic materials are produced because foreign materials are swept up by the migrating alumina. The establishment of the role of alumina in the sintering behaviour of these materials, therefore, will require further work, which ideally should include TEM observations at high temperature.

Acknowledgements

The authors thank Dr David Hay for the particle size determination by X-ray diffraction method and Mr David Watson for technical help.

References

1. R. C. GARVIE, R. H. J. HANNINK and R. T. PASCOE, *Nature* **258** (1975) 703.
2. N. CLAUSSEN and J. JAHN, *J. Amer. Ceram. Soc.* **61** (1978) 94.
3. P. BOCH and J. P. GIRY, *Mater. Sci. Engng* **71** (1985) 39.
4. M. OMORI, H. TAKEI and K. OHIRA, *J. Mater. Sci. Lett.* **4** (1985) 770.
5. F. F. LANGE and D. J. GREEN, in "Advances in Ceramics", Vol. 3, edited by A. H. Heuer and L. W. Hobbs (American Ceramic Society, 1981) p. 217.
6. A. H. HEUER, N. CLAUSSEN, W. M. KRIVEN and M. RÜHLE, *ibid.* **65** (1982) 642.
7. F. F. LANGE, US Pat. 4316964.
8. K. TSUKUMA and K. UEDA, *J. Amer. Ceram. Soc.* **68** (1985) C4.
9. S. RAJENDRAN, J. DRENNAN and S. P. S. BADWAL, *J. Mater. Sci. Lett.* **6** (1987) 1431.
10. S RAJENDRAN, M. V. SWAIN and H. J. ROSSELL, *J. Mater. Sci.* **23** (1988) 1805.
11. T. S. TOULOUKIAN, R. K. KIRBY, R. E. TAYLOR and T. Y. LEE, in "Thermal Expansion of Solids" (Plenum, 1977) p. 376.
12. K. WEFERS and G. M. BELL, Technical Paper no. 9, Alcoa Research Laboratories (1972) p. 39.
13. J. BANNISTER, *J. Aust. Ceram. Soc.* **18** (1982) 6.

Received 21 March
and accepted 28 July 1988